Fermi surface of Si(111)7×7

R. Losio, K. N. Altmann, and F. J. Himpsel
Department of Physics, UW-Madison, 1150 University Ave., Madison, Wisconsin 53706
and Synchrotron Radiation Center (SRC), 3731 Schneider Drive, Stoughton Wisconsin 53589
(Received 21 October 1999)

Surface states at the Si(111)7×7 surface are mapped by angle-resolved photoemission with E, ϑ multidetection. The adatom states near the Fermi level form a well-defined, two-dimensional energy surface consisting of closed loops that nearly fill the 7×7 unit cells. The width of the occupied adatom bands is 0.28 eV, twice as large as predicted by local density theory. Of the 49 possible locations inside the 1×1 cell, the loops centered at $\overline{\Gamma}_{7\times7}=(2/7,0)$ and $\overline{\Gamma}_{7\times7}=(3/7,-1/7)$ dominate in intensity, whereas those near (0,0) are suppressed by more than a factor of 20. These results provide quantitative input for characterizing narrow bands with substantial correlation effects at surfaces with large-scale reconstructions.

I. THE Si(111)7×7 SURFACE

The Si(111)7×7 surface has served as prototype of the complex atomic rearrangements that semiconductor surfaces undergo in order to minimize the number of broken bonds. A variety of structural studies in reciprocal and real space have established a highly refined structural model,[1–9] whose essential features are shown schematically in Fig. 1(a). Several mechanisms work in synergy for achieving the lowest density of broken bonds. The predominant energy lowering originates from adatoms which are connected to three broken bonds. Each adatom reduces three broken bonds to one, albeit at the expense of substantial strain [see Fig. 1(b)]. Thus, the 12 adatoms in the 7×7 unit cell remove nominally 24 broken bonds from a total of 49. An additional 6 broken bonds are removed by a change in stacking from staggered to eclipsed in half of the unit cell.[4–6] The boundaries between triangles of opposite stacking contain voids where broken bonds would be located on the unreconstructed surface. The combination of these two mechanisms leads to the Dimer Adatom Stacking fault model[7] of the 7×7 surface, which has been quantified by diffraction[7–9] and numerous other techniques. The large size of the 7×7 unit cell is determined by the triangular, faulted regions, which allow for odd × odd unit cells. The 7×7 cell optimizes the tradeoff between strain and bond density. It has been the goal of a variety of total energy calculations[10–20] to determine the surface energy and find out exactly why the 7×7 structure is the optimum.

The 19 broken bonds of the 7×7 unit cell form a 2×2 pattern inside each of its two triangular halves [Fig. 1(a)]. The corresponding structure factor gives rise to enhanced diffraction intensities for diffraction spots close to 2×2 positions. In addition to the 12 adatom bonds there are 6 broken bonds on the remaining surface atoms [often called rest atoms, see Fig. 1(b)]. The odd, 19th broken bond is similar to a rest atom, but located two layers deeper at the bottom of the corner hole of the 7×7 cell. Charge transfer[11] between adatoms and rest atoms provides an additional mechanism for lowering the energy. The 6 rest atoms are able to convert their half-filled broken bond orbitals into more stable lone pairs by extracting 6 electrons from the 12 adatoms. That leaves 6 electrons in the adatom orbitals, corresponding to 1/4 filling. In a band picture one would have a set of metallic adatom bands straddling the Fermi level, plus a completely filled set of rest atom bands. Even though the transfer of a full electron to the rest atoms seems large for a homopolar semiconductor, one should keep in mind that there is room for charge back donation via the back bonds, which reduces the net charge on the rest atoms. In addition, the environment of rest atoms and adatoms is quite different and makes them chemically dissimilar. The fate of the single orbital localized at the bottom of the corner hole is more difficult to predict. It might extract an extra electron from the adatoms, like the other rest atoms, and reduce the number of electrons in adatom orbitals to 5. Alternatively, the corner hole might give rise to an exotic, half-filled state with a low electron density of 1/49th of a monolayer.

Calculating the electronic structure of such a complex atom arrangement has been a challenge to the state of art in large-scale computation. Theoretical work[11,12,14–19,21–25] has suggested anything from localized orbitals to a delocalized band picture of model adatom structures.[11,14] In between these extremes lies the possibility of a correlated metal,[21,25] possibly displaying spin polarization.[24] The 7×7 structure should be metallic in a band picture, due to its odd number of electrons per unit cell. When correlations become sufficiently strong, the metallic surface might turn into a Mott insulator. Such a transition may occur if the on-site Coulomb repulsion U is larger than the band width W. That is a possibility for the 7×7 band structure.[25] The adatom orbitals are well-separated from each other, requiring electrons to hop across three intermediate atoms to get to an adjacent adatom. That leads to small hopping matrix elements between adatoms and to narrow adatom bands.

Available data on the electronic structure of the Si(111)7×7 surface have only hinted at a level of complexity comparable to that of the atomic structure. Photoemission studies[26–36] exhibit two nearly dispersionless surface states centered at 0.2 and 0.9 eV below the Fermi level. These have been assigned to the adatoms and rest atoms, respectively, by comparison with scanning tunneling spectroscopy.[37,38] Near the boundary of the 1×1 Brillouin zone a back-bond state has been found at 1.8 eV below the Fermi level. These three

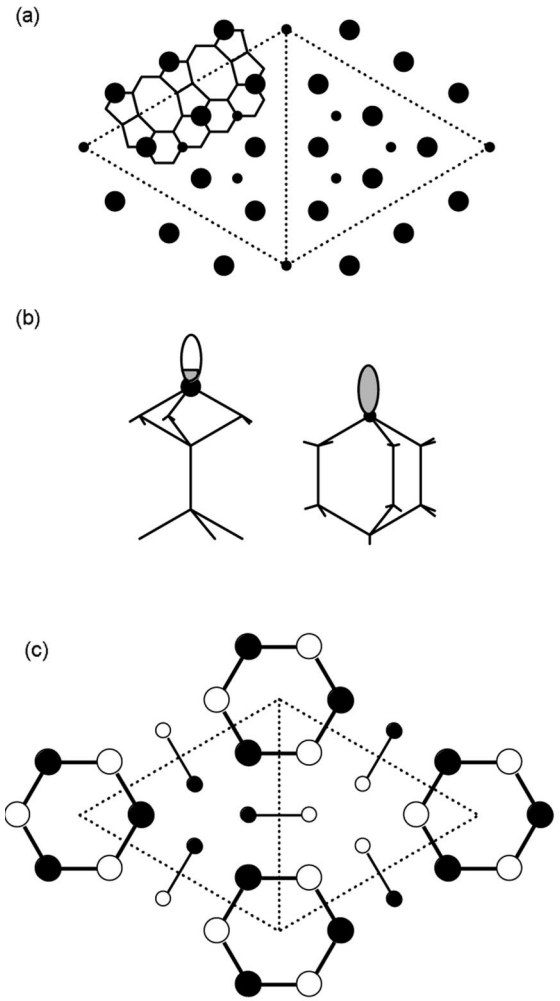

FIG. 1. The Si(111)7×7 surface structure. (a) Top view of the outermost double layer with adatoms shown as large dots and rest atoms as small dots. The bond topology of the outermost double layer is indicated in the upper left. (b) Side view of the bond geometry around an adatom and a rest atom. The adatoms transfer about $\frac{1}{2}$ electron each to the rest atoms, thereby filling the bond orbitals of the rest atoms and leaving the adatom orbitals $\frac{1}{4}$ occupied. (c) Grouping of the adatom states into nearly equivalent orbitals according to Ortega *et al.* (Ref. 25) with interactions between adatoms across a boundary between faulted and unfaulted triangles of the 7×7 structure.

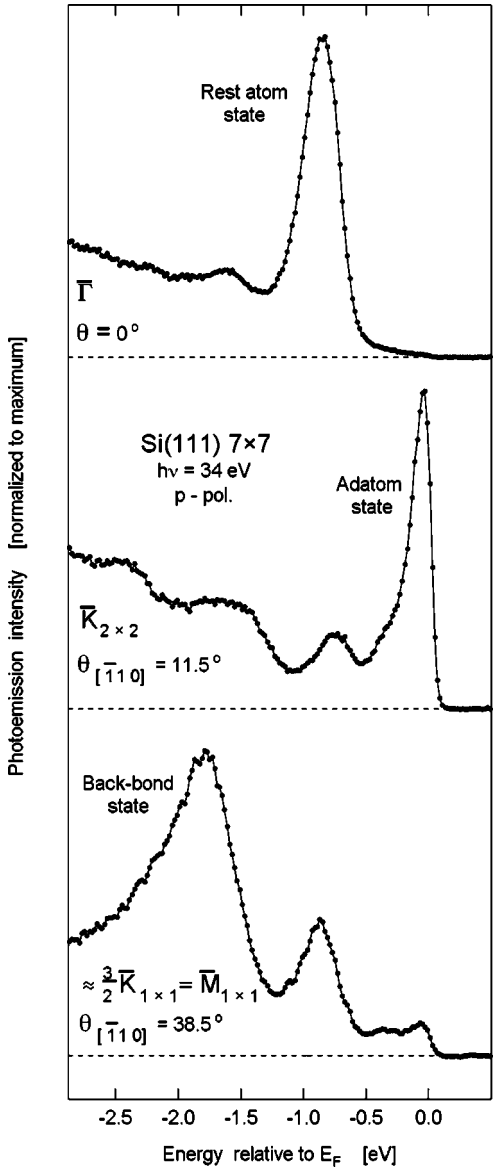

FIG. 2. The surface states of the Si(111)7×7 surface, brought out in photoelectron spectra at various emission angles. Partially filled adatom states dominate near the Fermi level, completely filled rest atom states are located near −0.8 eV, and back-bond states can be found near −1.8 eV. All energies are referenced to the pseudo Fermi level E_F, which is defined as the high energy cutoff of the angle-integrated spectrum at low temperature.

types of surface states can be clearly separated from each other and from the bulk states, as shown in Fig. 2. The rest atom states are completely occupied, indicating that they have picked up an extra electron. A weaker, third feature has been reported between these two states at low temperature and has been assigned to bonds located on the adatoms next to the corner holes.[36] The empty part of the adatom orbitals has been observed by inverse photoemission.[39–41] Transitions between filled and empty surface states have been measured by electron energy loss spectroscopy.[42–44] The loss energy varies rapidly from 1.0 to 1.7 eV for momentum transfers $\delta\mathbf{k}^{\parallel}$ within the small 7×7 surface Brillouin zone,[44] suggesting that there might be $E(\mathbf{k}^{\parallel})$ dispersion and fine structure of the broken bond orbitals that has escaped photoemission experiments. Likewise, the high-energy resolution achievable in electron energy loss spectroscopy has revealed sharp peaks at an energy loss δE of 63 and 95 meV at low temperature.[43]

The 7×7 surface has many hallmarks of a metallic surface at room temperature. Photoemission data exhibit intensity all the way to the Fermi level.[26–36] An asymmetric energy loss line is characteristic of infinitesimal transitions across a metallic Fermi level.[42,43] The surface Fermi level is strongly pinned[45,46] for both *p*-and *n*-type Si(111)7×7 indicating a substantial density of states near the Fermi level. The pinning position lies near the middle of the bulk band gap at 0.65 eV above the valence band maximum E_{VBM}.[45] When the temperature is lowered, the asymmetric background in the energy loss spectra gradually disappears around 100 K and gives way to sharp loss features at 20 K.[43]

These can be converted into an apparent gap of 40 meV by Kramers-Kronig analysis. This apparent gap has been interpreted in terms of a 2 meV wide, half-occupied state residing at the center of a 100 meV-wide gap.[43] Transport experiments have not been able to detect metallic surface conductivity on Si(111)7×7 at low temperatures.[47,48] A new look at the metallicity of the 7×7 surface was provided recently by a measurement of the temperature-dependent nuclear-spin relaxation rate of ^{8}Li probe atoms adsorbed on the 7×7 surface.[49] These results indicate a metallic surface, but with the correlation times increasing and the electron density decreasing to values that are borderline metallic when the temperature is reduced.

In view of the intriguing results about a possible metal-insulator transition at low temperature, the possibility of states as narrow as 2 meV, and a possible band dispersion on the momentum scale of the 7×7 Brillouin zone, it is desirable to perform photoemission measurements at low temperature with substantially higher energy and momentum resolution than in previous studies. Particularly important are the states closest to the Fermi level. They are responsible for electron-related transport properties and trigger a potential Mott transition. Even the very existence of a metallic Fermi surface is in question at low temperatures. A mapping of the two-dimensional Fermi surface has been attempted with low resolution, showing enhanced intensity of adatom states within 0.2 eV of the Fermi level near the boundaries of a 2×2 surface Brillouin zone.[31] Scans along high symmetry lines[27–33,35,36] are consistent with this finding. However, it is not clear whether the enhanced intensity reflects an enhanced cross section of a localized state, or whether it indicates the Fermi level crossing of a delocalized surface state band.

Using high-resolution photoemission with energy and angle multidetection we are able to resolve fine structure in the adatom states near the Fermi level at low temperatures. A two-dimensional emission pattern is found that consists of loops located just inside the circumference of the small 7×7 Brillouin zones. The loops shrink to points at the center of the 7×7 zone for an energy of −0.28 eV. The resulting width of the adatom bands is twice as large as expected from local density calculations and becomes consistent with theory only after taking electron correlations into account. Emission at the Fermi level is almost completely suppressed for the 7×7 zone centered at $\mathbf{k}=0$, suggesting that large-scale surface reconstructions should be described in $\mathbf{k}$ space by a nontraditional Brillouin zone scheme.

II. EXPERIMENT AND DATA ANALYSIS

Photoelectron spectra were acquired with a hemispherical Scienta spectrometer equipped with angle and energy multidetection. It was coupled to an undulator beam line with a plane grating monochromator (PGM) at the Synchrotron Radiation Center in Madison. Photon energies ranging from 22 to 48 eV were used with *p*-polarized photons incident 50° from the axis of the electron spectrometer. The energy resolution was 20 meV for the photons and 7 meV for the electrons. The angular resolution was about 0.3° full angle with the data taken in steps of 1° in [110] the direction ([112]) and every 0.24° in the angular multidetection direction, corresponding to about 50 channels over a 12° range.

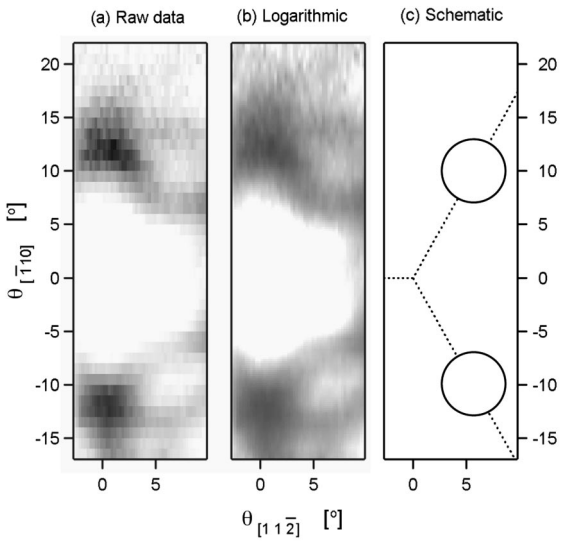

FIG. 3. Angular photoemission pattern from Si(111)7×7 at $h\nu = 34$ eV, showing the two-dimensional energy surface at the top of the adatom bands near the Fermi level. It contains two symmetric, faint loops, as indicated schematically in (c). High-photoemission intensity is shown dark.

The Si(111) samples were oriented with the $[\bar{1}10]$ azimuthal direction in the plane of incidence. The emission angles $\vartheta_{[\bar{1}10]}$ along the $[\bar{1}10]$ azimuth and $\vartheta_{[11\bar{2}]}$ along the orthogonal $[11\bar{2}]$ azimuth can be converted into the corresponding parallel wave vectors by

$$\mathbf{k}^{\parallel}_{[\bar{1}10]} = \hbar^{-1}(2mE_{\mathrm{kin}})^{1/2}\cdot\cos\vartheta_{[11\bar{2}]}\cdot\sin\vartheta_{[\bar{1}10]}$$

and

$$\mathbf{k}^{\parallel}_{[11\bar{2}]} = \hbar^{-1}(2mE_{\mathrm{kin}})^{1/2}\cdot\sin\vartheta_{[11\bar{2}]}.$$

Inside the limited angular range of Figs. 3 and 4 the approximations $\cos\vartheta_{[11\bar{2}]}\approx 1$ and $\sin\vartheta\approx\vartheta$ are valid within about 1% accuracy.

This geometry allowed us to cover a significant fraction of the 1×1 surface Brillouin zone with a grid dense enough to resolve fine structure within the small 7×7 Brillouin zone and to have an additional symmetry check with regard to the crystallographically-equivalent $[\bar{1}10]$ and $[1\bar{1}0]$ directions. Even though the $E(\mathbf{k})$ band dispersions along the $[\bar{1}10]$ and $[1\bar{1}0]$ directions are symmetric, the intensities are not. They correspond to different photon polarizations **A** and exhibit different photoemission matrix elements (see below). The $[11\bar{2}]$ and $[\bar{1}\bar{1}2]$ azimuths are not equivalent in the bulk, but nearly-symmetric for the 7×7 surface with its approximate six-fold symmetry. We find similar Fermi surfaces in both of these directions but with weaker intensity for $[\bar{1}\bar{1}2]$ (not shown).

In Fig. 4(d) we plot a variety of Brillouin zones together, since the Si(111)7×7 structure has been modeled by several smaller unit cells, such as $\sqrt{3}\times\sqrt{3}$ and 2×2. The wave vectors of the various symmetry points are: $\bar{K}_{1\times1} = 2\sqrt{2}/3\cdot 2\pi/a = 1.09\ \text{Å}^{-1}$; $\bar{M}_{1\times1} = \sqrt{2}/\sqrt{3}\cdot 2\pi/a$

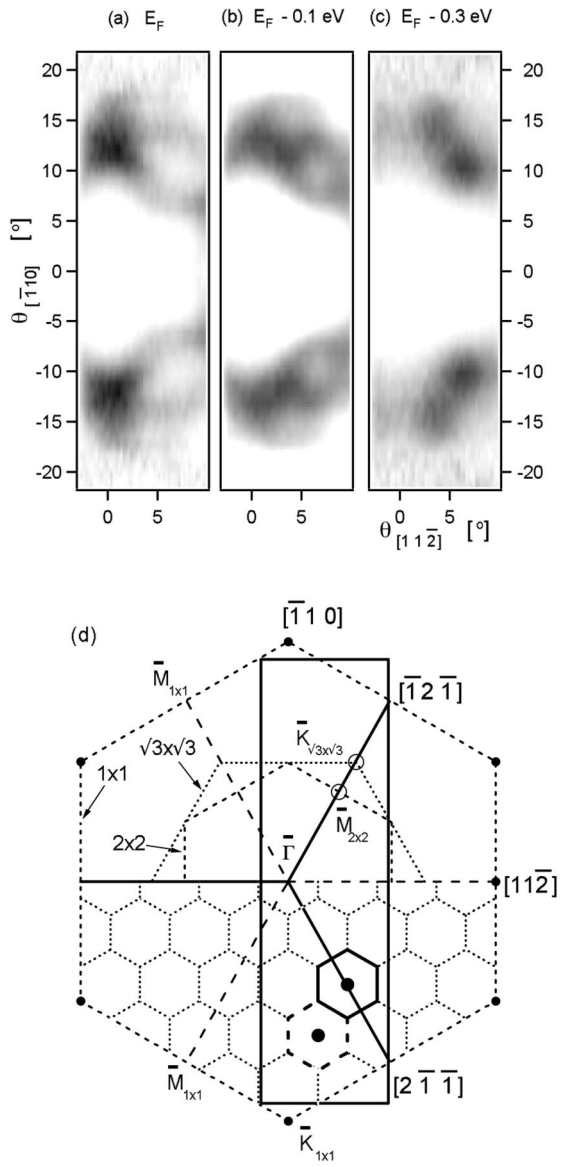

FIG. 4. Constant energy surfaces of Si(111)7×7 from angular photoemission patterns at various energies. The two loops near the Fermi level in (a) shrink at lower energy in (b) and contract into dark spots at the bottom of the band in (c). Neighboring loops appear in (b) and contract onto a separate pair of dark spots in (c). By overlaying the frames of (a)-(c) onto the rectangular box in (d) one can see that the Fermi surface lies just inside the boundary of a small, hexagonal 7×7 unit cell [shown bold in the bottom half of (d)]. The dark spots at the bottom of the band correspond to the centers of neighboring 7×7 unit cells [bold dots in (d)].

$=0.95\,\text{Å}^{-1}$; $\bar{K}_{\sqrt{3}\times\sqrt{3}}=0.63\,\text{Å}^{-1}$; $\bar{M}_{\sqrt{3}\times\sqrt{3}}=0.55\,\text{Å}^{-1}$; $\bar{K}_{2\times2}=0.55\,\text{Å}^{-1}$; $\bar{M}_{2\times2}=0.48\,\text{Å}^{-1}$; $\bar{K}_{7\times7}=0.16\,\text{Å}^{-1}$; $\bar{M}_{7\times7}=0.14\,\text{Å}^{-1}$.

The samples were *n*-type Si(111) stripes (0.02 Ωm, phosphorous-doped). They were clamped at their ends to a closed-cycle He refrigerator between sapphire plates and Ta contact sheets, which allowed for resistive heating. After an initial outgassing at temperatures up to 700 °C the samples were flashed to 1260 °C for 10 s where the native oxide evaporates and residual surface carbon diffuses into the bulk. A special cooling sequence was developed by monitoring the surface quality via scanning tunneling microscopy.[50] It ensures 7×7 domain sizes larger than 4000 Å for the 49 possible domains distinguished by different locations of the origin of the 7×7 cell. The most critical part of the cooling sequence is a quench below the 1×1 to 7×7 phase transition, in order to avoid step bunching, and a long post anneal at 850 °C to develop long-range 7×7 domains. The base pressure was below 5×10^{-11} Torr and rose briefly to 2×10^{-10} Torr during heat-cleaning.

The measurements were performed with the sample substrate at 16 K. At this temperature the illumination with intense synchrotron light caused a photovoltage[34,51] that shifted the high-energy cutoff of the spectrum down in energy by 0.47 eV relative to a Au reference sample at the same temperature. This photovoltage comes close to the saturation point, where the surface conduction band minimum shifts down until the band bending is eliminated. From the Fermi level pinning position[45] at 0.65 eV above the valence-band maximum E_{VBM} and from the band gap of 1.12 eV at room temperature one would expect a saturation photovoltage of 0.47 V for *n*-type samples. A more precise determination has to account for the larger band gap at low temperature (1.17 eV for <50 K), the exact Fermi level position in the bulk, and a possible change in the Fermi level pinning at low temperature.

An additional uncertainty in the position of the Fermi level is the possibility of a small gap in the surface state bands. Already at room temperature there are indications that the density of states decreases gradually towards the Fermi level, giving rise to a cutoff that is broader than the Fermi-Dirac function and shifted down in energy by 50–70 meV.[36] At low temperature this cutoff sharpens, and the density of states at the Fermi level is reduced. Our data are consistent with such a scenario, with the added photovoltage shifting both the surface states and the cutoff by the same amount (within 20 meV).

In order to have a reference level that is experimentally well defined we used the high energy cutoff in the angle-integrated photoelectron spectrum as a pseudo Fermi level E_F. All the figures refer to this cutoff. The real Fermi level may lie up to 70 meV higher. Likewise, the observed Fermi surface may describe the states at the bottom of a small gap.

The raw data on the Fermi surface of Si(111)7×7 consisted of about 50 energy spectra acquired in parallel during one scan over an angular range of 12°. The angular transmission function of the multidetector was carefully adjusted to exhibit minimal variations over the 12° detection range, with the analyzer deflection plates set close to zero voltage. Residual transmission variations were normalized out by taking a set of reference spectra at the same spectrometer settings, but 10 eV higher photon energy, where secondary electrons with little angular dependence are detected. Each reference spectrum was integrated over energy and then used to divide out the angular transmission function of the raw data. All spectra were normalized to the incident photon flux. A slow intensity variation with the angle of incidence ϑ was caused by a change of the areal photon density within the acceptance spot of the electron spectrometer. It was divided out as $\cos\vartheta$. Another slow variation was caused by the photoemission matrix element $|M_{fi}|^2\approx|\langle f|\mathbf{A}\cdot\mathbf{P}|i\rangle|^2$ between the initial state $|i\rangle$ and the final state $\langle f|$.[52] (**A** is the vector potential of

the photon, **P** the momentum operator.) All the surface states discussed here are predominantly excited by the component of **A** perpendicular to the surface ($A^{\perp}$), which would produce an intensity modulation of the form $|A^{\perp}|^2 \sim \sin^2\vartheta$ (to lowest order), where ϑ is again the angle of incidence relative to the sample normal. After dividing the intensity by the combination $\cos\vartheta \cdot \sin^2\vartheta$ we obtained a nearly mirror-symmetric intensity distribution for the adatom states in the crystallographically-equivalent $[\bar{1}10]$ and $[1\bar{1}0]$ azimuths [Figs. 3(a) and 3(b)]. The rest atom states remained asymmetric, indicating a more complex matrix element. In Figs. 4(a)–4(c) the photoemission patterns have been smoothened and symmetrized with respect to the *y*-axis such that they obey an exact $(1\bar{1}0)$ mirror plane symmetry.

For mapping the Fermi surface and band dispersion quantitatively in Fig. 5 we used angular intensity distributions analogous to those in Figs. 3 and 4 with the energy varied in steps of 60 meV. Radial profiles along the $[2\bar{1}\bar{1}]$ and $[\bar{1}2\bar{1}]$ azimuths show two Fermi level crossings [see Figs. 3 and 4(a)]. These were fitted by a pair of Gaussians, following a method developed for accurately determining band widths.[53] Only the peak positions and the combined intensities of the two Gaussians were varied, together with a background. The widths σ were held fixed with a linear energy dependence $\sigma(E) = a + b\cdot(E_F - E)$. The coefficients *a* and *b* were determined by a two-Gaussian fit at E_F [open triangles in Fig. 5(b)], and by a single-Gaussian fit below the bottom of the band [full triangles on the left side of Fig. 5(b)]. Likewise, the intensity ratio of the outer to the inner Fermi level crossing was kept fixed at 1.3. With these constraints it is possible to extract reliable positions for the energy contours even when they are starting to overlap as we go down in energy [Figs. 4(b) and 4(c)].

The bottom of the adatom bands at −0.28 eV was determined by three methods, which gave similar results ranging from −0.37 eV to −0.25 eV. First, the full width half maximum of the dark spots at the bottom of the band in Fig. 4(c) was determined as a function of energy [Fig. 5(b) full triangles]. Starting below the band, their width remains nearly constant until −0.28 eV, where it begins to increase sharply [fine arrow in Fig. 5(b)]. That suggests an electron pocket beginning to open up. The second method starts from above and measures the constant energy contours [compare the loops in Figs. 4(a) and 4(b)]. A parabolic fit in this regime [dashed line in Fig. 5(a)] gives values of from −0.28 to −0.25 eV for the bottom of the band, depending on the energy range of the fit. In both cases we are able to perform a symmetry check between the two equivalent $[\bar{1}2\bar{1}]$ and $[2\bar{1}\bar{1}]$ azimuths, which are represented by triangles pointing up and down in Fig. 5. A third signature of the bottom of the band is a small feature that appears at −0.37 eV in Fig. 2 (bottom) and at −0.30 eV in Fig. 2 (center).

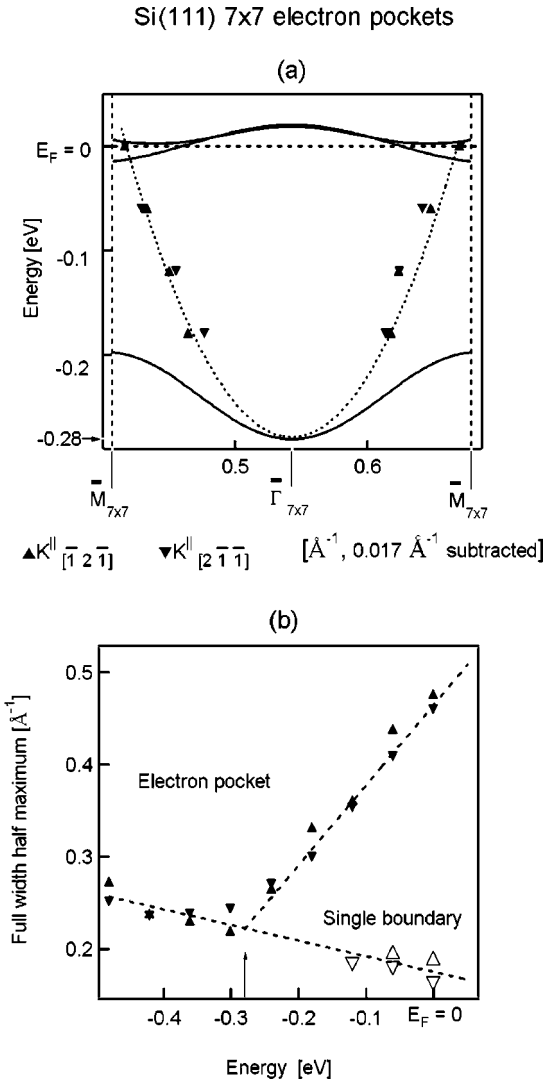

FIG. 5. Quantitative results on the adatom bands of Si(111)7×7 and comparison with theoretical models. (a) $E(\mathbf{k}^{\parallel})$ band dispersion for the two equivalent bands along the $[\bar{1}2\bar{1}]$ and $[2\bar{1}\bar{1}]$ azimuths (up and down triangles) obtained from a fit to a single, parabolic band (dashed line). The three occupied adatom bands predicted by local density theory (Ref. 25) are shown as full lines after stretching them by a factor of 2.2 in energy. (b) Width of the electron pockets near the bottom of the band (full triangles). A sudden increase at −0.28 eV indicates the bottom of the adatom bands.

III. ADATOM STATES AND FERMI SURFACE

The metallic character of the Si(111)7×7 surface is due to adatom states straddling the Fermi level. The Fermi cutoff observed in photoemission sharpens at low temperature due to the narrower Fermi-Dirac distribution. It also shifts downwards in energy due to a photovoltage that builds up as the carrier lifetime increases. This photovoltage effect is discussed in more detail in Sec. II. Our data are consistent with a metallic surface at low temperature, but we cannot exclude a small gap of the order 0.05–0.07 eV opening up.[36] In the following, the Fermi level E_F always designates the apparent high-energy cutoff of the spectra, but it is understood that the actual Fermi level could lie up to 0.07 eV higher.

For establishing a Fermi surface we plot the angular photoemission pattern at E_F [Fig. 3(a)]. High-photoemission intensity is shown in dark for better visibility. Even these raw data exhibit a well-defined fine structure that has not been observed before. The features are consistent with the crystal symmetry, where $\pm\vartheta_{[\bar{1}10]}$ are equivalent by mirror symmetry. Residual up-down asymmetries are due to the different orientation of the polarization vector for $\pm\vartheta_{[\bar{1}10]}$ (see Sec.

II). A smoothened, logarithmic plot of the same data in Fig. 3(b) covers the large dynamic range better. It exhibits two nearly-circular features that are represented schematically in Fig. 3(c). These loops lie 120° apart along the equivalent $[\bar{1}2\bar{1}]$ and $[2\bar{1}\bar{1}]$ azimuths of the (111) surface [dashed lines in Fig. 3(c)]. A mirror-symmetrized and smoothened version of the raw data is shown in Fig. 4(a). Additional data at -0.1 and -0.3 eV demonstrate a rapid change with energy, i.e., a strong $E(\mathbf{k})$ dispersion that has not been resolved previously. Minima at the center of the Fermi loops turn into maxima at -0.3 eV [dark spots in Fig. 4(c)]. In the following, we will discuss the overall intensity distribution first, then come to the topology of the Fermi surface, and eventually proceed to a quantitative analysis of the Fermi surface and band width.

Most of the photoemission takes place in a small fraction of the 1×1 Brillouin zone. This becomes obvious when using Fig. 4(d) as template for overlaying various surface Brillouin zones onto the data in Figs. 4(a)–4(c). Clearly, the 49 hexagons that form a honeycomb of 7×7 cells are not all equivalent to each other as far as the intensity is concerned. For example, the point $\bar{K}_{7\times7}=\pm4/7\bar{K}_{1\times1}$ is more than 20 times brighter than $\bar{K}_{7\times7}=\pm1/7\bar{K}_{1\times1}$, even though these points are equivalent in the 7×7 Brillouin zone. An equally dramatic intensity change can bee seen in Fig. 2 by comparing the top and middle spectrum at the Fermi level. This variation must be due to the photoemission matrix element[52] $|M_{fi}|^2\approx|\langle f|\mathbf{A}\cdot\mathbf{P}|i\rangle|^2$. Apart from the momentum operator $\mathbf{P}$ there are three components that can give rise to a modulation of the photoemission intensity in $\mathbf{k}$ space, i.e., the final state $\langle f|$, the $\mathbf{A}$ vector, and the initial state $|i\rangle$. The smooth variation of the $\mathbf{A}$ vector has been removed from the data already (see Sec. II). Final state effects can be tested by varying the photon energy $h\nu$. While the energy of the surface states remains unchanged at fixed $\mathbf{k}^{\|}$, there are large variations in the relative intensity of the adatom and rest atom states (not shown). The final state effect in photoemission may be viewed as photoelectron diffraction at the 7×7 lattice. More precisely, the final state in photoemission is the time-reversal of the state that describes low-energy electron diffraction (LEED).[52] It is well known that the LEED spots of the 7×7 surface exhibit a large structure factor near the half-order reflections[8] since the adatoms are arranged locally in a 2×2 structure. The initial state $|i\rangle$ can play a similar role, because its wave function contains strong 2×2 Fourier components as well. One way of finding out about this effect is the use of band calculations[14] for the 2×2 adatoms structure. They place a local minimum of the adatom band along the boundary of the 2×2 Brillouin zone with the bottom at $\bar{M}_{2\times2}$ [see Fig. 4(d) open circle]. Taking the occupied band width as a measure of the density of states available for photoemission one would expect the highest photoemission intensity near the boundary of the 2×2 zone [see Fig. 4(d)], in qualitative agreement with the observations. The intensity maximum of the Fermi surface near $\bar{K}_{2\times2}$ is likely to be caused by a coincidence of several factors: The Fermi surfaces of three adjacent 7×7 cells connect at this point, the structure factor is largest near the boundary of a 2×2 Brillouin zone, and the $\mathbf{A}\cdot\mathbf{P}$ matrix element has a maximum in the polarization plane ($\vartheta_{[11\bar{2}]}=0°$.)

The topology of the 7×7 Fermi surface has to follow the periodicity of the 7×7 honeycombs in Fig. 4(d), independent of strong intensity modulations. That can be tested by overlaying the emission patterns in Figs. 4(a)–4(c) onto the rectangular box in Fig. 4(d) and comparing them to the honeycomb of dotted 7×7 unit cells. A pair of faint Fermi loops is observed along the equivalent $[\bar{1}2\bar{1}]$ and $[2\bar{1}\bar{1}]$ azimuths [Fig. 4(a)]. They are centered at $\bar{\Gamma}_{7\times7}=4/7\bar{M}_{1\times1}=(2/7,0)$. These loops shrink in diameter at -0.1 eV [Fig. 4(b)], and close completely into spots at -0.3 eV[Fig. 4(c)]. The corresponding 7×7 cell is outlined as bold hexagon in Fig. 4(d). A similar, but weaker pair of loops appears at -0.1 eV in a neighboring 7×7 cell, which is centered at $\bar{\Gamma}_{7\times7}=(3/7,-1/7)$ using 1×1 basis vectors along the $[2\bar{1}\bar{1}]$ and $[11\bar{2}]$ directions. That cell corresponds to the heavy-dashed hexagon in Fig. 4(d). These weaker loops turn into to a second pair of spots in Fig. 4(c). All four spots observed at the bottom of the adatom band in Fig. 4(c) match the centers of 7×7 cells in Fig. 4(d)(filled dots weaker). That is consistent with band calculations for the 7×7 surface,[25] which find the bottom of the lowest adatom band at $\bar{\Gamma}_{7\times7}$. Thus, the fine structure of the Si(111)7×7 Fermi surface reflects the 7×7 periodicity in $\mathbf{k}$ space with the loops lying close to the circumference of the 7×7 cells, and the bottom of the band at the center.

A quantitative analysis of the Fermi surface and the band dispersion is presented in Fig. 5. For this purpose we have taken cuts of the photoemission intensity along the $[\bar{1}2\bar{1}]$ and $[2\bar{1}\bar{1}]$ azimuths which pass through the centers of the two most intense Fermi loops. A fitting routine described at the end of Sec. II allows us to extract an $E(\mathbf{k}^{\|})$ band dispersion [triangles in Fig. 5(a)] and an accurate position for the bottom of the band [Fig. 5(b) fine arrow]. The reliability of the data can be judged from a symmetry check between the equivalent $[\bar{1}2\bar{1}]$ and $[2\bar{1}\bar{1}]$ azimuths (triangles pointing up and down, respectively).

As the simplest interpretation of the data we show a parabolic fit as dashed line in Fig. 5(a). Such a single-band model gives an electron pocket centered at $k^{\|}=0.56\,\text{Å}^{-1}$. This location agrees with the center of a 7×7 Brillouin zone at $\bar{\Gamma}_{7\times7}=4/7\bar{M}_{1\times1}=0.54\,\text{Å}^{-1}$ within our absolute angular accuracy [compare Fig. 4(d), the full circle inside the bold hexagon]. For clarity we have shifted the data points by $0.017\ \text{Å}^{-1}$ in Fig. 5(a), such that they are centered at the exact location of the $\bar{\Gamma}_{7\times7}$ point. The center of this pocket lies between the points where band calculations for $\sqrt{3}\times\sqrt{3}$ and 2×2 model structures predict electron pockets [$\bar{M}_{2\times2}=0.48\,\text{Å}^{-1}$, $\bar{K}_{\sqrt{3}\times\sqrt{3}}=0.63\,\text{Å}^{-1}$; open circles in Fig. 4(d)]. The diameter of the electron pocket at the Fermi surface is $0.26\ \text{Å}^{-1}$, which comes close to the diameter of a 7×7 unit cell [$\bar{M}_{7\times7}\bar{\Gamma}_{7\times7}\bar{M}_{7\times7}=0.27\,\text{Å}^{-1}$, see the dashed vertical lines in Fig. 5(a)].

Such a simple one-band analysis cannot be the full answer. The band filling of 5–6 electrons requires at least $2\frac{1}{2}$ of the 12 adatom bands in a 7×7 unit cell to be occupied (see Sec. I). Therefore, we have to assume that the two other adatom bands are either suppressed in intensity or that our single parabola represents an unresolved set of three bands. In order to give a flavor of a more realistic band structure we

plot calculated 7×7 bands[25] in Fig. 5(a) as full lines. They had to be stretched by a factor of 2.2 in order to match the observed band width (more on that in Sec. V). In such a three-band interpretation one has small electron pockets centered at the 7×7 zone boundary $\overline{M}_{7\times7}$, instead of large pockets surrounding $\overline{\Gamma}_{7\times7}$. The data points at E_F in Fig. 5(a) are consistent with both interpretations. The shrinking of the Fermi loops below E_F in Fig. 4 seems to favor the single band explanation, but a closer look at the images expected from superimposing unresolved, multiple bands leaves the three-band model equally viable. The observation of a separate feature near −0.3 eV in Fig. 2 (center and bottom) favors multiple bands.

IV. REST ATOM STATES

The rest atom states form a lone pair when considering them as localized orbitals. In a band picture one expects a completely filled surface state band, which is indeed what one finds (see Fig. 2). There is a small, but measurable $E(\mathbf{k}^{\|})$ band dispersion of 0.16 eV from −0.87 eV at $\overline{\Gamma}_{1\times1}$ to −0.71 eV near $\overline{K}_{1\times1}$. It demonstrates that this state is somewhat delocalized. The width of the adatom state (0.3 eV FWHM) is larger than the dispersion, but its non-Lorentzian line shape indicates that it consists of unresolved subbands. From the lone pairs at the 6 rest atoms in the 7×7 cell one expects 6 fully occupied adatom bands, plus an additional band from the corner hole atom. The fact that the band dispersion does not follow the 7×7 periodicity suggest a strong modulation of the subband intensities similar to the matrix element effects discussed in Sec. III for the adatom bands. Instead of going into details of the rest atom bands we focus onto the adatom states at the Fermi level, which have a much larger impact on the theoretical understanding of the Si(111)7×7 surface.

V. IMPLICATIONS ON THEORETICAL MODELS

A variety of theoretical models have been used to describe the electronic structure, starting either from an atomic orbital picture of broken bonds or from a band picture for delocalized electrons. Recent calculations explore the uncharted territory in between, where the band structure is strongly affected by electron correlation effects. We will proceed in this order and discuss how our data eliminate some of these concepts and put constraints on others.

Localized orbital models of the Si(111)7×7 bands can be disposed of rather quickly by our observations. The fact that we are measuring a significant band dispersion shows clearly that a description in terms of sharp energy levels is inadequate. This conclusion is reinforced by our observation of a band that crosses the Fermi level and forms a 7×7-like Fermi surface.

In a band model of the Si(111)7×7 surface states, one expects a metallic surface because of the odd number of electrons per 7×7 unit cell. The 19 broken bonds provide 19 electrons that are to be distributed among the rest atom and adatom bands. Assuming lone pairs on the 6 rest atoms plus the corner atom, one has to place 14 electrons into 7 rest atom bands that are completely filled. The remaining 5 electrons are to be distributed among 12 adatom bands. Such a program has been carried out by local density theory.[25]

Before discussing such a complex set of bands it is useful to consider simpler band calculations where the electronic characteristics of the 7×7 structure are derived from smaller unit cells, such as a $\sqrt{3}\times\sqrt{3}$ structure[11] that contains only a single adatom per unit cell, and a 2×2 structure[14] that contains one adatom and one rest atom. The 2×2 structure replicates the atomic arrangement on each of the triangular halves of the 7×7 cell [see Fig. 1(a)]. Local density calculations for both unit cells give an adatom band that has its minimum at the Brillouin zone boundary along the $[\overline{1}2\overline{1}]$ azimuth, which corresponds to $\overline{K}_{\sqrt{3}\times\sqrt{3}}$ and $\overline{M}_{2\times2}$ [see open circles in the top half of Fig. 4(d)]. This is exactly the region where we find the brightest part of the Fermi surface. That suggests that a modulation of the initial state wave function by the local 2×2 adatom structure plays an important role in determining the photoemission cross section. The $\sqrt{3}\times\sqrt{3}$ and 2×2 models have their shortcomings, however. The $\sqrt{3}\times\sqrt{3}$ structure is metallic with a half-filled adatom band, but it lacks rest atoms. The 2×2 structure contains both kinds of atoms, but is semiconducting. Its single adatom transfers an electron to the single-rest atom, leading to an empty adatom band. In neither case one comes close to the proper band filling of $\frac{5}{12}$ for the adatom bands of the 7×7 structure.

The band width is the principal characteristic of band models. We distinguish the combined width of all adatom bands and the width of their occupied portion, which is accessible to photoemission. Local density calculations give a total band width of 0.44, 0.25, and 0.37 eV for the $\sqrt{3}\times\sqrt{3}$, 2×2, and 7×7 structure.[11,14,25] In order to obtain a meaningful occupied band width one would have to adjust the position of the Fermi level for the $\sqrt{3}\times\sqrt{3}$ and 2×2 structures to the occupancy factor $\frac{5}{12}$ of the 7×7 surface. Simply rescaling the total band width by the occupancy gives rough estimates of 0.18 and 0.10 eV for the occupied band width of the 7×7 surface from the $\sqrt{3}\times\sqrt{3}$ and 2×2 calculations. The full 7×7 calculation comes up with a similar value of 0.13 eV for the occupied adatom bands.[25] These numbers are to be compared to our experimental band width of 0.28 eV, which is twice as large [compare Fig. 5(a), where the local density bands had to be stretched by a factor of two in order to match the experiment]. This result is reminiscent of other narrow band systems, such as the F2p valence band of LiF, where local density theory underestimates the band width as well.[54]

The effective mass at the bottom of the adatom bands is a second parameter that can be compared to theory. It comes out close to unity in local density calculations for all three unit cells ($\sqrt{3}\times\sqrt{3}$, 2×2, and 7×7), whereas our data give an effective mass of 0.23 when interpreted as a single band [see Fig. 5(a), dashed line]. After correcting for the factor of two in the bandwidth discrepancy, there is still another factor of two discrepancy in the effective mass. That may be an indication that we are observing a superposition of several unresolved bands, such as the three adatom bands expected from local density calculations for the 7×7 structure [full lines in Fig. 5(a)].

The effect of correlations is rather complex for a unit cell

as large as 7×7. Nevertheless, it has been possible to perform first principles band calculations and to add correlation effects, such as an on-site Coulomb interaction U and several other types of Coulomb interactions between the charges sitting on adatoms and rest atoms.[25] The end result of the many-body calculations is an increased band width that comes close to the observations. Thus, it appears that correlations have a significant effect on the adatom states (they double the band width), but that they do not destroy the band picture altogether. The metallic character derived from the odd number of electrons per unit cell is preserved, at least at room temperature. For analogous surfaces with overlayers[55–62] however, a complete breakdown of the band picture and the electron counting rule has been reported.

VI. CONCLUSIONS AND OUTLOOK

In conclusion, we have resolved two-dimensional energy surfaces for Si(111)7×7 that contain fine structure corresponding to the long-range 7×7 periodicity. The energy surface closest to the Fermi level lies just inside the boundaries of 7×7 unit cells. While this observation is consistent with the Fermi surface predicted by band calculations, the width of all occupied adatom bands is twice as large as in local-density theory. Such a large band width can be explained qualitatively by on-site and off-site Coulomb interactions introducing correlations between dangling bond electrons.[25] The photoemission intensity is strongly modulated by 2×2 Fourier components of the initial and final state wave functions, which leads to a radical distortion of the intensity distribution among different 7×7 cells. That suggests a rethinking of how to view the band structure and Fermi surface for unit cells as large as 7×7. Even the very existence of a Fermi surface remains in question. There could be a small gap Δ of the order of 50–70 meV below the Fermi level, similar to that observed in low-dimensional charge density waves.[63,64] In that case our data correspond to a pseudo Fermi surface that describes the states at the bottom of the gap. Even more exotic effects are predicted for the 7×7 surface, such as a Kondo-like peak only a few meV wide.[25]

ACKNOWLEDGMENTS

We would like to acknowledge A. Kaminski, H. Fretwell, and J. C. Campuzano for the use of their cryostat and help with setting up the experiment. We have benefited from discussions with José Ortega on theoretical models of the Si(111)7×7 surface. This work was supported by the NSF under Award Nos. DMR-9815416 and DMR-9632527. It was conducted at the SRC, which is supported by the NSF under Award No. DMR-9531009.

[1] R. E. Schlier and H. E. Farnsworth, J. Chem. Phys. **30**, 917 (1959).
[2] W. A. Harrison, Surf. Sci. **55**, 1 (1976).
[3] G. Binnig, H. Rohrer, Ch. Gerber, and E. Weibel, Phys. Rev. Lett. **50**, 120 (1983).
[4] F. J. Himpsel, Phys. Rev. B **27**, 7782 (1983).
[5] E. G. McRae, Phys. Rev. B **28**, 2305 (1983).
[6] P. A. Bennett, L. C. Feldman, Y. Kuk, E. G. McRae, and J. E. Rowe, Phys. Rev. B **28**, 3656 (1983).
[7] K. Takayanagi, Y. Tanishiro, M. Takahashi, and S. Takahashi, J. Vac. Sci. Technol. A **3**, 1502 (1985); K. Takayanagi, Y. Tanishiro, S. Takahashi, and M. Takahashi, Surf. Sci. **164**, 367 (1985).
[8] S. Y. Tong, H. Huang, C. M. Wei, W. E. Packard, F. K. Men, G. Glander, and M. B. Webb, J. Vac. Sci. Technol. A **6**, 615 (1988).
[9] I. K. Robinson, W. K. Waskiewicz, P. H. Fuoss, and L. J. Norton, Phys. Rev. B **37**, 4325 (1988).
[10] J. E. Northrup and M. L. Cohen, Phys. Rev. B **29**, 1966 (1984).
[11] J. E. Northrup, Phys. Rev. Lett. **57**, 154 (1986).
[12] G.-X. Qian and D. J. Chadi, Phys. Rev. B **35**, 1288 (1987).
[13] D. Vanderbilt, Phys. Rev. B **36**, 6209 (1987).
[14] R. D. Meade and D. Vanderbilt, Phys. Rev. B **40**, 3905 (1989).
[15] G. B. Adams and O. F. Sankey, Phys. Rev. Lett. **67**, 867 (1991).
[16] I. Stich, M. C. Payne, R. D. King-Smith, J.-S. Lin, and L. J. Clarke, Phys. Rev. Lett. **68**, 1351 (1992).
[17] K. D. Brommer, M. Needels, B. E. Larson, and D. J. Joannopoulos, Phys. Rev. Lett. **68**, 1355 (1992); K. D. Brommer, M. Needels, B. E. Larson, M. Needels, and D. J. Joannopoulos, Jpn. J. Appl. Phys., Part 1 **32**, 1360 (1993); K. D. Brommer, M. Galván, A. Dal Pino, and D. J. Joannopoulos, Surf. Sci. **314**, 57 (1994); H. Lim, K. Cho, I. Park, D. J. Joannopoulos, and E. Kaxiras, Phys. Rev. B **52**, 17 231 (1995).
[18] J. Kim, M.-L. Yeh, F. S. Khan, and J. W. Wilkins, Phys. Rev. B **52**, 14 709 (1995).
[19] D. R. Alfonso, C. Noguez, D. A. Drabold, and S. E. Ulloa, Phys. Rev. B **54**, 8028 (1996).
[20] V. Khavryutchenko, E. Sheka, M. Aono, and D. H. Huang, Phys. Low-Dimens. Semicond. Struct. **11/12**, 1 (1996).
[21] E. Louis, F. Flores, F. Guinea, and C. Tejedor, Solid State Commun. **44**, 1633 (1982).
[22] M. Fujita, H. Nagayoshi, and A. Yoshimori, Surf. Sci. **242**, 229 (1991).
[23] L. Stauffer, S. Van, D. Bolmont, J. J. Koulmann, and C. Minot, Solid State Commun. **85**, 935 (1993); L. Stauffer, P. Sonnet, and C. Minot, Surf. Sci. **371**, 63 (1997).
[24] V. Khavryutchenko, E. Sheka, D. H. Huang, and M. Aono, Phys. Low-Dimens. Semicond. Struct. **3/4**, 81 (1998).
[25] J. Ortega, F. Flores, and A. L. Yeyati, Phys. Rev. B **58**, 4584 (1998); J. Ortega, A. L. Yeyati, and F. Flores, Appl. Surf. Sci. **123/124**, 131 (1998); J. Ortega, F. Flores, R. Pérez, and A. L. Yeyati, Prog. Surf. Sci. **59**, 233 (1998).
[26] J. E. Rowe and H. Ibach, Phys. Rev. Lett. **32**, 421 (1974).
[27] D. E. Eastman, F. J. Himpsel, J. A. Knapp, and K. C. Pandey, Inst. Phys. Conf. Ser. **43**, 1059 (1979).
[28] G. V. Hanson, R. I. G. Uhrberg, and S. A. Flodström, J. Vac. Sci. Technol. **16**, 1287 (1979).
[29] F. Houzay, G. M. Guichar, R. Pinchaux, P. Thiry, Y. Petroff, and D. Dagneaux, Surf. Sci. **99**, 28 (1980).
[30] T. Yokotsuka, S. Kono, S. Suzuki, and T. Sagawa, Solid State Commun. **39**, 1001 (1981).
[31] F. J. Himpsel, D. E. Eastman, P. Heimann, B. Reihl, C. W. White,

and D. M. Zehner, Phys. Rev. B **24**, 1120 (1981). More recent angular distribution patterns of surface states on Si(111)7×7 have been obtained with a similar display spectrometer by J. Terry, L. J. Terminello, *et al.* (unpublished).

[32] H. Neddermeyer, U. Misse, and P. Pupieper, Surf. Sci. **117**, 405 (1982).

[33] R. I. G. Uhrberg, G. V. Hansson, J. M. Nicholls, P. E. S. Persson, and S. A. Flodström, Phys. Rev. B **31**, 3805 (1985).

[34] J. E. Demuth, W. J. Thompson, N. J. DiNardo, and R. Imbihl, Phys. Rev. Lett. **56**, 1408 (1986).

[35] P. Martensson, W.-X. Ni, G. V. Hansson, J. M. Nicholls, and B. Reihl, Phys. Rev. B **36**, 5974 (1987).

[36] R. I. G. Uhrberg, T. Kaurila, and Y.-C. Chao, Phys. Rev. B **58**, R1730 (1998); In this study, the Fermi level is placed 50–70 meV higher than our pseudo Fermi level.

[37] R. J. Hamers, R. M. Tromp, and J. E. Demuth, Phys. Rev. Lett. **56**, 1972 (1986).

[38] R. Wolkow and Ph. Avouris, Phys. Rev. Lett. **60**, 1049 (1988).

[39] F. J. Himpsel and Th. Fauster, J. Vac. Sci. Technol. A **2**, 815 (1984).

[40] J. M. Nicholls and B. Reihl, Phys. Rev. B **36**, 8071 (1987).

[41] F. J. Himpsel, Surf. Sci. Rep. **12**, 1 (1990).

[42] U. Backes and H. Ibach, Solid State Commun. **40**, 575 (1981).

[43] J. E. Demuth, B. N. J. Persson, and A. Schell-Sorokin, Phys. Rev. Lett. **51**, 2214 (1983).

[44] J. M. Layet, J. Y. Hoarau, H. Lüth, and J. Derrien, Phys. Rev. B **30**, 7355 (1984).

[45] F. J. Himpsel, G. Hollinger, and R. A. Pollak, Phys. Rev. B **28**, 7014 (1983); This earlier result gives $E_F - E_{\mathrm{VBM}} = 0.63 \pm 0.05\,\mathrm{eV}$ for Si(111)7×7. A more accurate value is $E_F - E_{\mathrm{VBM}} = 0.65\,\mathrm{eV}$ from: F. J. Himpsel, B. S. Meyerson, F. R. Mc Feely, J. F. Morar, A. Taleb-Ibrahimi, and J. A. Yarmoff, in ''*Photoemission and Absorption Spectroscopy of Solids and Interfaces with Synchrotron Radiation*,'' edited by M. Campagna and R. Rosei (North Holland, Amsterdam, 1990), p. 203.

[46] J. Viernow, M. Henzler, W. L. O'Brien, F. K. Men, F. M. Leibsle, D. Y. Petrovykh, J. L. Lin, and F. J. Himpsel, Phys. Rev. B **57**, 2321 (1998).

[47] R. Schad, S. Heun, T. Heidenblut, and M. Henzler, Phys. Rev. B **45**, 11 430 (1992).

[48] S. Hasegawa, Z. H. Zhang, C. S. Jiang, and S. Ino, Springer Series in Materials Sciences, Vol. 31, edited by H. Sakaki and H. Noge (Springer, Berlin, 1994), p. 330.

[49] D. Fick, R. Veith, H. D. Ebinger, H. J. Jänsch, C. Weindel, H. Winnefeld, and J. J. Paggel, Phys. Rev. B **60**, 8783 (1999).

[50] J. Viernow, J.-L. Lin, D. Y. Petrovykh, F. M. Leibsle, F. K. Men, and F. J. Himpsel, Appl. Phys. Lett. **72**, 948 (1998); J.-L. Lin, D. Y. Petrovykh, J. Viernow, F. K. Men, D. J. Seo, and F. J. Himpsel, J. Appl. Phys. **84**, 255 (1998).

[51] P. Pervan, K. Market, and K. Wandelt, Appl. Surf. Sci. **108**, 307 (1997).

[52] F. J. Himpsel, Adv. Phys. **32**, 1 (1983).

[53] I. Jiménenz, L. J. Terminello, D. G. J. Sutherland, J. A. Carlisle, E. L. Shirley, and F. J. Himpsel, Phys. Rev. B **56**, 7215 (1997).

[54] F. J. Himpsel, L. J. Terminello, D. A. Lapiano-Smith, E. A. Eklund, and J. J. Barton, Phys. Rev. Lett. **68**, 3611 (1992); E. L. Shirley, L. J. Terminello, J. E. Klepeis, and F. J. Himpsel, Phys. Rev. B **53**, 10296 (1996).

[55] H. H. Weitering, J. Chen, N. J. DiNardo, and E. W. Plummer, Phys. Rev. B **48**, 8119 (1993); H. H. Weitering, X. Shi, P. D. Johnson, J. Chen, N. J. DiNardo, and K. Kempa, Phys. Rev. Lett. **78**, 1331 (1997).

[56] J. M. Carpinelli, H. H. Weitering, E. W. Plummer, and R. Stumpf, Nature (London) **381**, 398 (1996).

[57] J. M. Carpinelli, H. H. Weitering, M. Bartkowiak, R. Stumpf, and E. W. Plummer, Phys. Rev. Lett. **79**, 2859 (1997).

[58] A. Mascaraque, J. Avila, E. G. Michel, and M. C. Asensio, Phys. Rev. B **57**, 14 758 (1998).

[59] J. Avila, A. Mascaraque, E. G. Michel, M. C. Asensio, G. LeLay, J. Ortega, R. Pérez, and F. Flores, Phys. Rev. Lett. **82**, 442 (1999).

[60] V. Ramachandran and R. M. Feenstra, Phys. Rev. Lett. **82**, 1000 (1999).

[61] G. Santoro, S. Scandolo, and E. Tosatti, Phys. Rev. B **59**, 1891 (1999).

[62] F. Flores, J. Ortega, and R. Pérez, Surf. Rev. Lett. **6**, 411 (1999).

[63] M. Grioni, I. Vobornik, F. Zwick, and G. Margaritondo, J. Electr. Spectrosc. **100**, 313 (1999).

[64] H. W. Yeom, S. Takeda, E. Rotenberg, I. Matsuda, K. Horikoshi, J. Schaefer, C. M. Lee, S. D. Kevan, T. Ohta, T. Nagao, and S. Hasegawa, Phys. Rev. Lett. **82**, 4898 (1999).